

Beware of CaBER: Filament thinning rheometry does not always give ‘the’ relaxation time of polymer solutions

A. Gaillard^a, M. A. Herrada^b, A. Deblais^a, J. Eggers^c, D. Bonn^a

^a*Van der Waals-Zeeman Institute, University of Amsterdam, Science Park 904, Amsterdam, Netherlands*

^b*Depto. de Mecánica de Fluidos e Ingeniería Aeroespacial, Universidad de Sevilla, Sevilla, E-41092, Spain*

^c*School of Mathematics, University of Bristol, University Walk, Bristol, BS8 1 TW, United Kingdom*

Abstract

The viscoelastic relaxation time of a polymer solution is often measured using Capillary Breakup Extensional Rheometry (CaBER) where a droplet is placed between two plates which are pulled apart to form a thinning filament. For a slow plate retraction protocol, required to avoid inertio-capillary oscillations for low-viscosity liquids, we show experimentally that the CaBER relaxation time τ_e inferred from the exponential thinning regime is in fact an apparent relaxation time that may increase significantly when increasing the plate diameter and the droplet volume. Similarly, we observe that τ_e increases with the plate diameter for the classical step-strain plate separation protocol of a commercial (Haake) CaBER device and increases with the nozzle diameter for a Dripping-onto-Substrate (DoS) method. This dependence on the flow history before the formation of the viscoelastic filament is in contradiction with polymer models such as Oldroyd-B that predict a filament thinning rate $1/3\tau$ (τ being the model’s relaxation time) which is a material property independent of geometrical factors. We show that this is not due to artefacts such as solvent evaporation or polymer degradation and that it can only be rationalised by finite extensibility effects (FENE-P model) for a dilute polymer solution in a viscous solvent, but not for semi-dilute solutions in a low-viscosity solvent.

Keywords: Viscoelasticity; Polymers; Capillary flows

1. Introduction

When polymers are added to a low-viscosity solvent such as water, the extensional rheology of the resulting solution is usually measured by indirect techniques where the (exten-

*Corresponding author

Email address: antoineogaillard@gmail.com (A. Gaillard)

sional) strain and strain rate are not controlled, unlike for high-viscosity polymer solutions or melts for which reliable extensional rheometers are available, e.g. Meissner’s RME (Rheometric Melt Elongation rheometer) and FiSER (Filament Stretching Extensional Rheometer). Most indirect techniques for low-viscosity polymer solutions aim at forming a liquid filament undergoing capillary-driven thinning. Historically, this was first achieved by placing a drop of liquid between two horizontal plates which are then separated beyond the stability limit of a stable liquid bridge [1–3], a technique now known as CaBER (Capillary Breakup Extensional Rheometry). Alternative techniques, also based on the Rayleigh-Plateau instability, were proposed to avoid inertio-capillary oscillations of the end-drops in the original CaBER step-strain (rapid) plate separation protocol which prohibits measurement of very short relaxation times [4]. This is achieved by separating the plates at a constant low velocity (Slow Retraction Method or SRM) [5], by dripping a droplet in air from a nozzle at a low flow rate [6] or, in a more recent technique, by slowly bringing a solid substrate in contact with a drop hanging steadily from a nozzle (Dripping-onto-Substrate or DoS) [7].

In all these techniques, after an initial inertial and/or viscous regime, an elastic regime emerges where the elastic stresses arising from the stretching of polymer chains dominate and give rise to a cylindrical filament that thins exponentially in time for a wide range of dilute and semi-dilute polymer solutions. This is consistent with the Oldroyd-B model that predicts [8, 9]:

$$h = h_1 \exp\left(-\frac{t - t_1}{3\tau}\right), \quad (1)$$

where h is the minimum filament radius, τ the viscoelastic relaxation time of the polymer solution, t_1 the time marking the onset of the elastic regime, and $h_1 = h(t_1)$ the filament radius at that time. For a step-strain CaBER protocol, in which polymer molecules do not relax during the fast plate separation, the model predicts $h_1 = (Gh_i^4/2\gamma)^{1/3}$ where $G = \eta_p/\tau$ is the elastic modulus, η_p the polymer contribution to the shear-viscosity, γ the surface tension and h_i the radius of the initial liquid column [10]. It is generally accepted that (i) for a polymer solution with a spectrum of relaxation times, the longest one dominates [2] and that (ii) as polymer chains unravel during the exponential regime, they ultimately approach their finite extensibility limit, causing the filament to break after a terminal regime which can be described by, e.g., FENE models (P or CR) [2, 9, 11].

The general consensus is that geometrical parameters such as the size of the system can only influence h_1 (via h_i) but not the thinning rate $|\dot{h}/h| = 1/3\tau$ of the filament (where the dot means d/dt) since τ is a material property. In particular, Bazilevsky et al. [1] and Miller et al. [12] checked that the filament thinning rate was independent of the sample volume and of the plate separation speed and, in a step-strain plate separation protocol, on the final plate separation distance. This suggests that it is independent of the history of the polymer deformation prior to the elastic regime. However, Rajesh et al. [13] recently

Name	ρ (kg/m ³)	γ (mN/m)	η_s (mPa s)	c (ppm)	c/c^*	η_0 (mPa s)	η_p (mPa s)	n	$1/\dot{\gamma}_c$ (ms)	τ_m (ms)
PEO _{aq}	998	62.5	0.92	500	1.86	3.0	2.08	0.93	120	240
PEO _{visc}	1048	56.0	245	25	0.018	248	3.3	1	–	110
HPAM	998	72.0	0.92	1000	–	15	14	0.78	410	100

Table 1: Properties of the three polymer solutions. ρ is the density, γ the surface tension, η_s the solvent viscosity, c the polymer concentration, c^* the critical overlap concentration, η_0 , n and $\dot{\gamma}_c$ the Carreau fitting parameters of the shear viscosity, $\eta_p = \eta_0 - \eta_s$, and τ_m the maximum CaBER relaxation time measured for the largest plates.

tested polymer solutions of different solvent viscosities with a dripping method and reported a larger thinning rate for a smaller nozzle radius.

In this paper, we show that the apparent relaxation time, inferred from the exponential thinning regime, depends on the size of the system for other filament thinning techniques such as CaBER (with both slow and fast plate separation protocols) and Dripping-onto-Substrate (DoS).

2. Materials and methods

2.1. Polymer solutions

We use three different liquids: two solutions of poly(ethylene oxide) (PEO) of molecular weight $M_w = 4 \times 10^6$ g/mol, one in water with concentration 500 (w)ppm, referred to as PEO_{aq}, and one in a more viscous solvent with concentration 25 (w)ppm, referred to as PEO_{visc}, and a 1000 ppm solution of poly(acrylamide/sodium acrylate) (HPAM) [70:30] of molecular weight $M_w = 18 \times 10^6$ g/mol in water with 1 wt% NaCl to screen electrostatic interactions and make the chain flexible instead of semi-rigid. Both polymers were provided by Polysciences (ref. 04030-500 for PEO and 18522-100 for HPAM). For the PEO_{visc} solution, the solvent is an aqueous Newtonian 30 wt% 20,000 g/mol PEG solution. The different concentrations were chosen to ensure that all three liquids have comparable filament thinning rates. After slowly injecting the polymer powder to a vortex generated by a magnetic stirrer, solutions were homogenised using a mechanical stirrer at low rotation speed for about 16 hours. For the PEO_{visc} solution, PEG was added after mixing PEO with water.

The shear viscosity η of these solutions was measured at the temperature of filament thinning experiments with a MRC-302 rheometer from Anton Paar equipped with a cone plate geometry (diameter 50 mm, angle 1° and truncation gap 53 μ m). The PEO_{visc} solution is a Boger fluid with a constant shear viscosity while the two others are shear-thinning and are well described by the Carreau law $\eta(\dot{\gamma}) = \eta_0(1 + (\dot{\gamma}/\dot{\gamma}_c)^2)^{(n-1)/2}$ where η_0 is the zero-shear viscosity,

n is the shear-thinning exponent and $\dot{\gamma}_c$ is the shear rate marking the onset of shear thinning. These values, along with the solvent viscosity η_s , the density ρ and the surface tension γ measured with a pendent drop method, are reported in table 1. For the PEO_{aq} (500 ppm) solution, viscosity measurements for other PEO concentrations gave an intrinsic viscosity $[\eta] = 2.87 \text{ m}^3/\text{kg}$ and hence a critical overlap concentration $c^* = 0.77/[\eta] = 0.268 \text{ kg}/\text{m}^3$ (268 ppm). Assuming that the PEO_{visc} solution (25 ppm) is dilute, η_p should increase linearly with the concentration as $\eta_p = [\eta]\eta_s c$, from which $[\eta]$ and c^* are estimated from this single PEO concentration. Values of c/c^* are presented in table 1.

2.2. Slow stepwise plate separation CaBER protocol

In our home-made CaBER setup, a droplet of volume V is placed on a horizontal plate of radius R_0 and the motor-controlled top plate of same radius is first moved down until it is fully wetted by the liquid, i.e., until the liquid bridge between the plates has a quasi cylindrical shape. The top plate is then moved up slowly (at about 0.5 mm/s) and stopped at a plate separation distance L_p where the liquid bridge is still stable, like in the left inset image of figure 1(a), but close to the bridge instability threshold. Then, instead of moving the top plate at a constant (lower) velocity, i.e. like in SRM [5], we move it by $10 \mu\text{m}$ L_p -increment steps, waiting about one second between each step (longer than the solution's relaxation time), which is long enough to ensure that polymers are at equilibrium (no pre-stress) before each new step. At a certain step, the bridge becomes unstable and collapses under the action of surface tension, transiently leading to the formation of a nearly cylindrical filament which is the signature of viscoelastic pinch-off, as shown in the right inset image of figure 1(a). We stop moving the top plate once capillary-driven thinning starts. The CaBER setup is placed in a plastic box where the relative humidity is kept above 80% using wet paper to minimise evaporation. The aluminium plates are plasma-treated before each new experiment to increase their hydrophilicity and minimise dewetting.

The process is recorded by a high-magnification objective mounted on a high-speed camera (Phantom TMX 7510) and images are analysed by a python code. A typical time-evolution of the minimum bridge / filament radius h is shown in figure 1(a). The purpose of this step-by-step plate separation protocol is to extract the value of the last stable bridge radius h_0 which, since steps are small, can be considered as the initial bridge radius at the onset of capillary thinning. Our image resolution is up to 1 pixel per micrometer for the smallest drops, corresponding to the smallest plates, and our time resolution is 15,000 images per second to capture the fast bridge collapse from radius h_0 to the radius h_1 marking the onset of the elastic regime, see figure 1(a).

The critical aspect ratio $\Lambda = L_p/(2R_0)$ at which the liquid bridge becomes unstable depends on the liquid volume V and on the Bond number $Bo = \rho g R_0^2/\gamma$, where g is the gravitational acceleration [14]. In our experiments, we vary both the plate diameter $2R_0$,

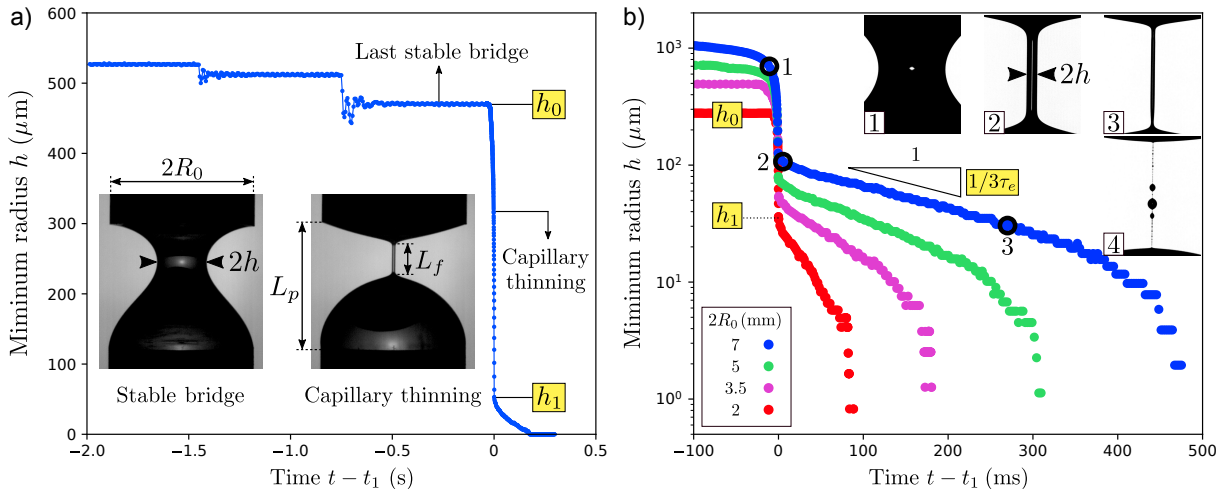


Figure 1: (a) Time evolution of the minimum bridge / filament radius h in the slow stepwise plate separation protocol for the PEO_{aq} solution for plate diameters $2R_0 = 3.5$ mm and a droplet volume $V^* = V/R_0^3 \approx 2.4$. Inertio-capillary oscillations are visible after each step. Inset images correspond to a stable liquid bridge (left) and to a thinning filament (right) of the PEO_{aq} solution with $2R_0 = 7$ mm and $V^* \approx 2.4$. (b) $h(t)$ in log-lin for the PEO_{aq} solution tested with plate diameters, $2R_0 = 2, 3.5, 5$ and 7 mm, with $V^* \approx 2.4$. Inset images correspond to three times labelled 1 to 3 indicated on the $h(t)$ curve plus a fourth later time where h is below our spatial resolution for $2R_0 = 7$ mm. The time reference t_1 marks the onset of the elastic regime.

between 2 and 25 mm, and the non-dimensional droplet volume $V^* = V/R_0^3$ and we find that the last stable bridge radius h_0 increases with both R_0 and V^* .

3. Results

Figure 1(b) compares the time-evolution of the minimum bridge / filament radius h for the PEO_{aq} solution tested with plate diameters $2R_0$ between 2 and 7 mm with a fixed non-dimensional droplet volume $V^* = V/R_0^3 \approx 2.4$. Although all filaments thin exponentially in time at the beginning of the elastic regime, as suggested by the fairly straight curves for $t > t_1$ (before the terminal regime), they thin faster for smaller plates. This is in apparent contradiction with the Oldroyd-B model, which predicts a rate of exponential thinning $|\dot{h}/h| = 1/3\tau$ (see equation 1) which should be the same for all filaments, provided that the liquid does not change so that the (longest) relaxation time τ of the polymer solution is the same.

To quantify these differences, we introduce an apparent (or effective) relaxation time τ_e such that $|\dot{h}/h| = 1/3\tau_e$ in the exponential part of the elastic regime. As figure 1(b) suggests, τ_e increases as the plate diameter increases. We show similar results for a Dripping-onto-Substrate (DoS) method in Appendix A, where τ_e is found to increase with the nozzle

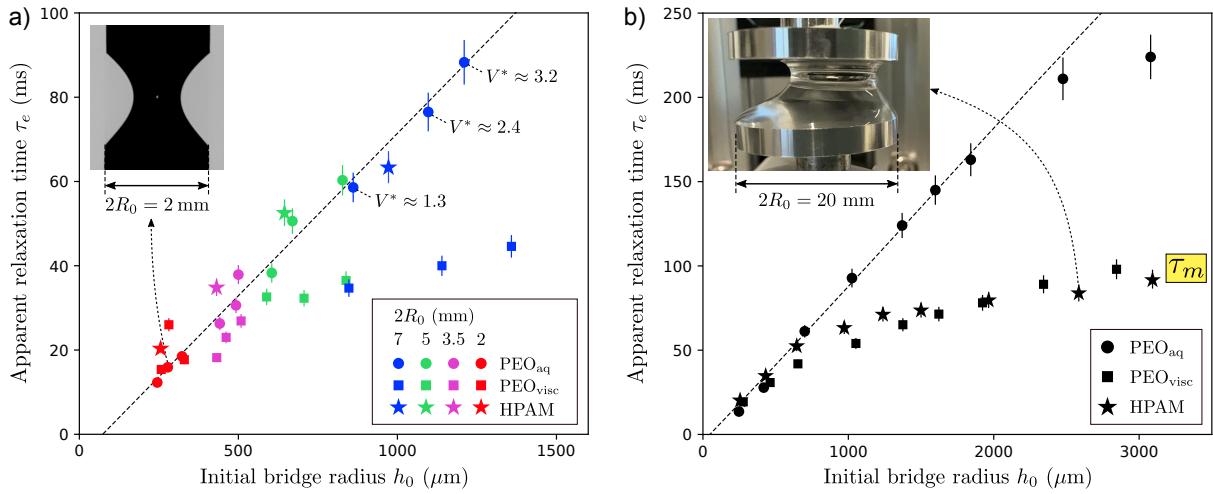


Figure 2: Apparent relaxation time τ_e against h_0 for all three solutions for plate diameters $2R_0 = 2, 3.5, 5$ and 7 mm (a) and for $2R_0 = 2, 3.5, 5, 7, 10, 12.5, 15, 20$ and 25 mm (b). In (a), data points of the same colour correspond to the same R_0 with different droplet volumes $V^* = V/R_0^3 \approx 1.3, 2.4$ and 3.2 (only $V^* \approx 2.4$ for the HPAM solution). In (b), a single volume is used for each plate diameter ($V^* \approx 2.4$ for the smallest plates and 0.88 for the largest plates). The inset images show stable liquid bridges for $2R_0 = 2$ mm (a) and 20 mm (b). The linear fit is for the PEO_{aq} solution for $h_0 < 2$ mm.

diameter. In Appendix B, we also show similar results for the classical step-strain plate separation protocol of a commercial (Haake) CaBER device where τ_e is found to increase with the plate diameter. This suggests a universal physical mechanism for the dependence of the filament thinning rate on the size of the system, independent of the exact method used.

The apparent relaxation time τ_e measured with our slow stepwise plate separation CaBER protocol is plotted in figure 2(a) as a function of the initial bridge radius h_0 for various plate diameters and droplet volumes for all three polymer solutions, data points of the same colour corresponding to the same R_0 with different V^* . We observe that τ_e increases with both R_0 and V^* and that all data points for a given solution collapse on a single curve when plotted against h_0 , which is itself an increasing function of both R_0 and V^* . In other words, a given solution tested with two different (R_0, V^*) sets but with the same h_0 yields the same τ_e , as some examples show in figure 2(a). This suggests that h_0 is in fact the only relevant geometrical parameter of the problem. This is in agreement with the accepted idea that polymer deformations during capillary thinning are only influenced by the local extensional flow in the bridge / filament of maximum extension rate $\dot{\epsilon} = -2\dot{h}/h$ at its thinnest point, while the top and bottom end droplets act as passive liquid reservoirs, their size not directly influencing the pinch-off dynamics.

The apparent relaxation time varies significantly (up to a factor 4) within the typical

range of plate diameters used for CaBER experiments, see figure 2(a). However, τ_e cannot increase indefinitely with increasing h_0 . In order to observe the expected saturation of τ_e for larger h_0 values, we had to move to much larger plate diameters, up to $2R_0 = 25$ mm. For plate diameters $2R_0 \geq 10$ mm, the top end-drop does not cover the top plate fully because of gravity, as shown in the inset image of figure 2(b). In fact, there is always a thin liquid film covering the top plate due to the plasma treatment. For such large plates, the top end-drop is not at the centre of the the top plate since the two plates are not perfectly parallel.

In spite of this lack of full coverage for large plates, we find that the critical minimum bridge radius h_0 marking the onset of the Rayleigh-Plateau instability increases with R_0 , allowing us to explore a wider range h_0 values, as shown in figure 2(b) where the apparent relaxation time τ_e seems to saturate to a maximum value τ_m , reported in table 1, at large h_0 . Since no clear plateau is observed, especially for the PEO_{aq} solution, the value of τ_m is only an estimation. In figure 2(b), we only show one data point for each plate diameter, with V^* between 2.4 for the smallest plates and 0.88 for the largest plates. Note that no change in behaviour is observed in the $\tau_e(h_0)$ curves in figure 2(b) at the transition between fully covered ($2R_0 \leq 7$ mm) and not fully covered top plates ($2R_0 \geq 10$ mm), around $h_0 \approx 1.3$ mm, strengthening the claim that the top and bottom end-drops are passive liquid reservoirs whose size and shape do not affect the filament thinning dynamics.

As shown by the inset images in figure 2(a,b), the bottom end-drop becomes increasingly larger than the top one as R_0 increases since the Bond number $Bo = \rho g R_0^2 / \gamma$ ranges between 0.16 and 25. However, the thinning dynamics is not driven by gravity since the “filament” Bond number $Bo_f = \rho g L_f h_1 / \gamma$, comparing the typical capillary pressure γ / h_1 in the filament to the hydrostatic pressure $\rho g L_f$ over the filament length L_f , is only up to 0.1 for the largest plates. This is also evident from the fact that filaments are not thicker at their base, see, e.g., the right inset image in figure 1(a). This is consistent with the fact that, as we discuss in our longer companion paper [15], the bridge thinning dynamics is well captured by the classical inertio-capillary and visco-capillary (gravity-free) self-similar laws (close to the transition to the elastic regime) for the PEO_{aq} and PEO_{visco} solutions, respectively, for plate diameters where τ_e depends on h_0 (hence suggesting that the h_0 -dependence of τ_e is not caused by gravitational drainage). These apparent extensional relaxation times τ_e are compared with relaxation times inferred from shear rheology in our companion paper [15].

Note that the PEO solutions used in figures 2(b) are not the same as the ones used in figure 2(a) and have apparent relaxation times about 30% larger for $2R_0 = 7$ mm, while the shear viscosity was only up to 10 % larger, meaning that the shear rheology parameters in table 1 are representative of both solutions. These differences are due to slightly different preparation protocols, e.g. agitation times, for a given recipe. These extra solutions were prepared because, by the time we had realised much larger plates were needed to observe the saturation of τ_e , the previous solutions had considerably aged, i.e., had lower τ_e values.

4. Interpretations

The apparent disagreement between experiments and equation 1 implies that either the liquid changes, becoming less elastic for lower values of h_0 , or that the Oldroyd-B model, from which equation 1 is derived, misses some important features of polymer dynamics in extensional flows. We now consider some possible explanations.

4.1. Evaporation and degradation

First, although the relaxation time measured in filament thinning is known to increase with polymer concentration [6, 11], solvent evaporation cannot explain the observed increase of the apparent relaxation time with increasing droplet size. Indeed, the bulk polymer concentration would increase quicker for smaller droplets due to their larger surface to volume ratio, leading to larger concentrations for smaller droplets, and hence larger τ_e , while the opposite is observed (lower τ_e for lower h_0). Besides, repeating an experiment several times over the course of 10 minutes does not lead to a monotonic increase or decrease of τ_e over time, beyond small variations of less than 5%. This is not surprising since humidity is kept at high levels ($> 80\%$) in the CaBER chamber. The latter observation also argues against polymer degradation as a possible explanation. Moreover, τ_e is observed to increase with h_0 for both PEO and HPAM solutions, even though HPAM is less fragile than PEO.

Therefore, if the liquid is in fact the same for each experiment, the Oldroyd-B model fails to describe the full polymer dynamics in the bridge / filament. In particular, differences in the history of polymer deformations for different drop sizes could lead to different “initial” states of polymers at the onset of the elastic regime, which could result in different filament thinning rates. We now discuss whether finite extensibility of polymer chains, as described by the FENE-P model, can account for such differences.

4.2. Elasto-capillary balance with FENE-P

Following Wagner et al. [16], for a uniaxial extensional flow, the polymeric part of the normal stress is $\sigma_{p,zz} = G(fA_{zz} - 1)$ in the flow direction z where G is the elastic modulus and A_{zz} is the normal part of the conformation tensor \mathbf{A} which follows

$$\dot{A}_{zz} - 2\dot{\epsilon}A_{zz} = -\frac{fA_{zz} - 1}{\tau}, \quad (2)$$

where $\dot{\epsilon}$ is the extension rate, τ the relaxation time and $f = (1 - \text{tr}(\mathbf{A})/L^2)^{-1}$ where L is the ratio of the fully unravelled chain size to its equilibrium size. In this model the stress diverges as A_{zz} approaches its limit value L^2 .

In the elastic regime ($t \geq t_1$), we assume that polymers are far from equilibrium and that the axial stress dominates over the radial stress, i.e. $A_{zz} \gg 1 > A_{rr}$. Assuming negligible

inertia and solvent viscosity in the elastic regime, we use the elasto-capillary force balance equation

$$(2X - 1)\frac{\gamma}{h} = \sigma_{p,zz} = GfA_{zz}, \quad (3)$$

with $f = (1 - A_{zz}/L^2)^{-1}$ where $X = 3/2$ in the Oldroyd-B limit [17]. Assuming a small correction due to finite extensibility, combining equations 2 and 3 with $\dot{\epsilon} = -2\dot{h}/h$ leads to the ordinary differential equation $(3 + A_{zz}/L^2)\dot{A}_{zz} = A_{zz}/\tau$ which has an implicit solution

$$\frac{t - t_1}{\tau} = \frac{A_{zz} - A_1}{L^2} + 3 \ln \left(\frac{A_{zz}}{A_1} \right), \quad (4)$$

where $A_1 = A_{zz}(t_1)$ quantifies the amount of polymer stretching at the onset of the elastic regime at time t_1 . The filament radius can be computed by noticing that hfA_{zz} is a constant according to equation 3, i.e.

$$\frac{h}{h_1} = \frac{f_1 A_1}{f A_{zz}}, \quad (5)$$

where $f_1 = (1 - A_1/L^2)^{-1}$ and $h_1 = h(t_1)$ is the filament radius at the onset of the elastic regime. h depends on three parameters: τ , h_1 and the ratio A_1/L^2 quantifying how far chains are from being fully extended at the onset of the elastic regime. Indeed, according to equations 4 and 5, h is unchanged upon multiplying both A_1 and L^2 by the same quantity. In the Oldroyd-B limit $L^2 \rightarrow \infty$ ($f = 1$), we recover the expected exponential trends $A_{zz} = A_1 \exp((t - t_1)/3\tau)$ and $h = h_1 \exp(-(t - t_1)/3\tau)$. For a finite extensibility, the exponential regime holds until A_{zz} approaches L^2 where finite extensibility effects arise. Ultimately, the stress diverges and $h \rightarrow 0$ in finite time when A_{zz} saturates to L^2 , which occurs sooner as A_1/L^2 is closer to one. In particular, if A_1/L^2 is only slightly less than 1, meaning that polymer chains are already almost fully extended at the onset of the elastic regime, finite extensibility effects are never negligible and equation 1 is never valid. In that case, increasingly larger filament thinning rates are observed as A_1/L^2 increases and equations 4 and 5 predict that the apparent relaxation time τ_e is well approximated by $\tau_e/\tau \approx 1 - A_1/L^2$.

This theory is tested in figure 3(a) where the elastic regime ($t \geq t_1$) of the PEO_{aq} solution, tested with different plate diameters, is compared with the predictions of equations 4 and 5 where we have chosen the maximum relaxation time τ_m (table 1) measured at large h_0 as the relaxation time of the FENE-P model. We use A_1/L^2 and h_1 as fitting parameters to obtain a good agreement between model and experiments. Most importantly, we have to impose that A_1/L^2 gets closer to one as h_0 decreases to capture the observed thinning rates, all larger than $1/3\tau_m$. For $2R_0 = 2$ mm for example, we need $A_1/L^2 = 0.93$, meaning that polymers are almost fully extended at the onset of the elastic regime.

We emphasise here that in previous studies, where τ_e was believed to not vary with the plate size, comparisons with the FENE-P model were performed using τ_e as the model's

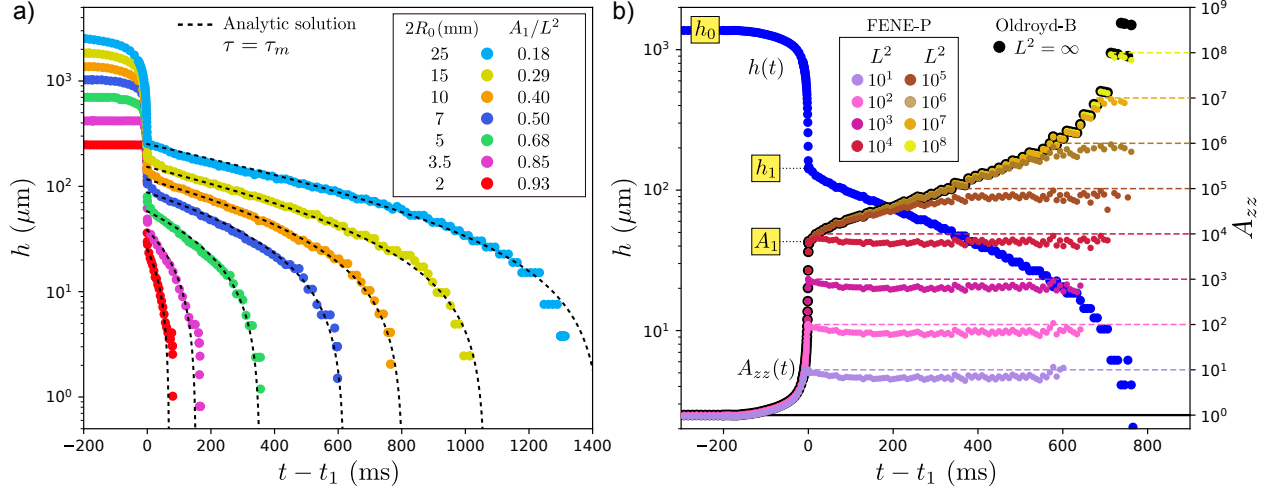


Figure 3: (a) Experimental $h(t)$ for the PEO_{aq} solution tested with different plate diameters. The elastic regime ($t \geq t_1$) is fitted by equation 4 and 5 with relaxation time $\tau = \tau_m$ (from experiments, table 1), using h_1 and A_1/L^2 as fitting parameters. Fitting values of the parameter A_1/L^2 are given in the legend. (b) Experimental $h(t)$ for the PEO_{aq} solution tested with a single plate diameter $2R_0 = 10$ mm and corresponding values of $A_{zz}(t)$ calculated from equation 2 with $\dot{\epsilon} = -2\dot{h}/h$ using the experimental values of h , with relaxation time $\tau = \tau_m$ (from experiments, table 1) where we vary the value of L^2 from 10 to 10^8 (FENE-P) and $L^2 = \infty$ (Oldroyd-B), using $A_{zz} = 1$ at $h = h_0$ as the initial condition. The Ohnesorge numbers $Oh = \eta_0/\sqrt{\rho\gamma h_0}$ ranges between 0.02 and 0.007 for the PEO_{aq} solution in our range of h_0 values which corresponds to plates diameters $2R_0$ between 2 and 25 mm.

relaxation time, and it is quite remarkable that when using a larger value τ_m , one can still obtain a somehow exponential-looking trend with the right thinning rate by tuning A_1/L^2 for $\tau_e < \tau_m$. Equally good fits can be obtained for the PEO_{visc} and HPAM solutions and the corresponding values of the fitting parameter A_1/L^2 are plotted against h_0 in figure 4(a) (light purple). These results suggest that the maximum relaxation time τ_m measured at large plate sizes could be the ‘true’ relaxation time, lower apparent values τ_e being a consequence of polymers being too close to their finite extensibility limit at the onset of the elastic regime to display their ‘natural’ (far from full extension) relaxation behaviour.

4.3. Calculating $A_{zz}(t)$ from experimental $h(t)$ with FENE-P

In §4.2, we used A_1/L^2 as a fitting parameter and showed that it should increase towards 1 as h_0 decreases in order to successfully describe the elastic regime. However, values of A_1 can in fact be calculated from the flow history in the Newtonian regime ($t < t_1$). Therefore, we now check the consistency of the proposed interpretation for the variation of τ_e with h_0 by calculating A_1 from the FENE-P model, examining whether polymers are indeed expected to be more stretched at the onset of the elastic regime for smaller plate diameters or not.

To this end, we use equation 2 to calculate $A_{zz}(t)$, using the experimental values of $h(t)$ for $\dot{e}(t) = -2\dot{h}/h$, although this expression is only valid at the thinnest bridge radius. In other words, we calculate the predictions of the model for the experimental history of extension rates. In particular, the extension rate history in the Newtonian regime ($t < t_1$) sets A_1 . Hence, we do *not* assume large polymer deformations ($A_{zz} \gg 1$) since, as our slow stepwise plate separation protocol is designed for, polymers are at equilibrium at the onset of capillary thinning, i.e. $A_{zz} = 1$ when $h = h_0$. We use $f = (1 - A_{zz}/L^2)^{-1}$ since when f is not close to 1 anymore, the axial stress dominates over radial stress. In order to circumvent the issue of calculating \dot{h} from experimental values of h , we introduce a function $y(t)$ such that $A_{zz} = y/h^4$, which gives $\dot{A}_{zz} + 4(\dot{h}/h)A_{zz} = \dot{y}/h^4$, so that equation 2 becomes $\tau\dot{y} = h^4 - y/(1 - y/(h^4L^2))$ which does not involve \dot{h} anymore. To solve this equation, we use a standard ODE solver, using spline interpolation to create a $t \rightarrow h(t)$ function based on experimental values of h . This equation can be integrated analytically in the Oldroyd-B limit, as shown by Bazilevsky et al. [18].

The results are shown in figure 3(b) for the PEO_{aq} solution tested with a plate diameter $2R_0 = 10$ mm, with $\tau = \tau_m$ (table 1) for the relaxation time of the FENE-P model, along with various values of L^2 , including the Oldroyd-B limit $L^2 \rightarrow +\infty$. As expected, values of A_{zz} calculated from FENE-P coincide with Oldroyd-B until it saturates when reaching L^2 . In particular, the value of A_1 becomes independent of L^2 when L^2 is sufficiently large and becomes indistinguishable from the values predicted by the Oldroyd-B model.

4.4. Comparing fitting and calculated A_1 values

The values of $A_1 = A_{zz}(t_1)$ calculated in §4.3 from the experimental values of $h(t)$ in the Newtonian regime ($t < t_1$), using the FENE-P model with $\tau = \tau_m$, are plotted in figure 4(a) against h_0 for all three solutions (dark blue). More precisely, we plot the ratio A_1/L^2 indicating how close polymer chains are to being fully extended at the onset of the elastic regime (full extension corresponding to $A_1/L^2 = 1$). This is because we want to compare these calculated values (dark blue) with the values of A_1/L^2 used as a fitting parameter (light purple) in §4.2 to fit the elastic regime with equations 4 and 5 (see figure 3(a)). We hence need to choose a value of L^2 . For each liquid, we choose L^2 such that, at the largest h_0 , the calculated value (dark blue) of A_1/L^2 coincides exactly with the fitting value (light purple). We obtain $L^2 = 4.9 \times 10^4$ for the PEO_{aq} solution, $L^2 = 2.0 \times 10^4$ for the PEO_{visc} solution and $L^2 = 6.2 \times 10^3$ for the HPAM solution. The order of magnitude is consistent with the microscopic formula [11]

$$L^2 = 3 \left[\frac{j \sin^2(\theta/2) M_w}{C_\infty M_u} \right]^{2(1-\nu)}, \quad (6)$$

which gives L^2 between 4.5×10^4 and 1.3×10^5 for PEO of molecular weight $M_w = 4 \times 10^6$ g/mol, for typical solvent quality exponents ν between 0.55 and 0.5 (theta solvent) found

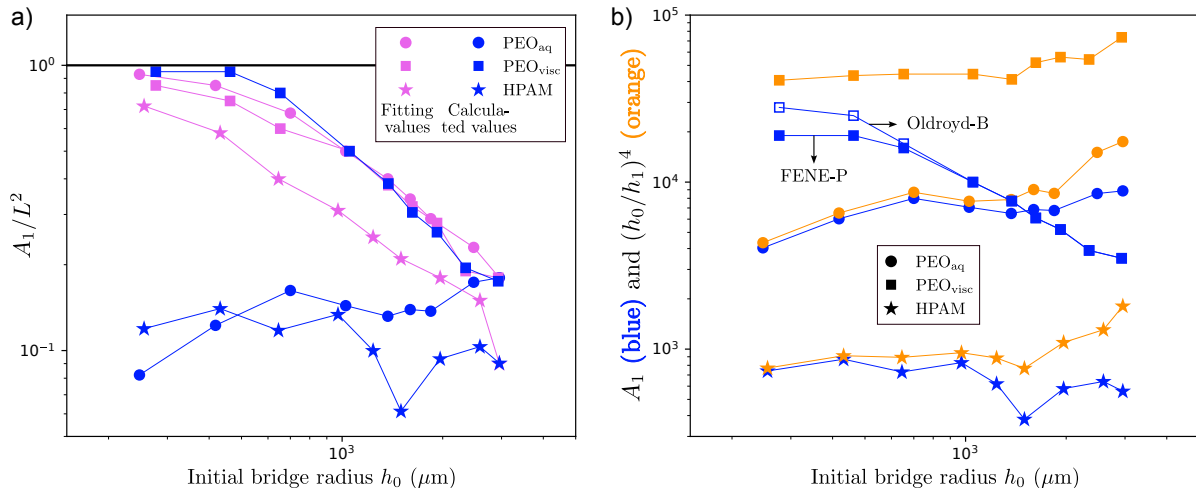


Figure 4: (a) Values of A_1/L^2 used as fitting parameters (light purple, see e.g. figure 3(a)), and values calculated from the FENE-P model (dark blue, see e.g. figure 3(b)) for $\tau = \tau_m$ and values of L^2 discussed in the text, against h_0 for all liquids and plate diameters. (b) Same values of A_1 calculated from the FENE-P model (dark blue), compared with $(h_0/h_1)^4$ (light orange). All values of A_1 calculated from FENE-P are the same as in Oldroyd-B except for the PEO_{visc} solution at low h_0 where Oldroyd-B values are shown with empty blue symbols. The Ohnesorge numbers $Oh = \eta_0/\sqrt{\rho\gamma h_0}$ ranges between 0.02 and 0.007 for the PEO_{aq} solution, between 0.1 and 0.03 for the HPAM solution and between 2 and 0.6 for the PEO_{visc} solution in our range of h_0 values which corresponds to plates diameters $2R_0$ between 2 and 25 mm.

for PEO in water-based solvents, where M_u is the monomer molecular weight, $\theta = 109^\circ$ the C-C bond angle, $j = 3$ the number of bonds of a monomer and $C_\infty = 4.1$ the characteristic ratio [19]. We find that, while the fitting values of A_1 (light purple) increase towards L^2 as h_0 decreases, the calculated values of A_1 (dark blue) only do so for the PEO_{visc} solution, for which a good agreement is found with the fitting values, and do not for the PEO_{aq} and HPAM solutions for which A_1 is fairly constant. For these last two, no other value of L^2 can lead to a better agreement since decreasing L^2 would just shift all calculated values towards the upper limit $A_1/L^2 = 1$.

In order to better understand this, we compare these calculated values of A_1 (dark blue) with their upper limit $(h_0/h_1)^4$ (light orange) in figure 4(b). This upper limit corresponds to a relaxation time τ so large that polymer relaxation (right hand side of equation 2) is always negligible in the Newtonian regime ($t < t_1$), a case where equation 2 (with $\dot{\epsilon} = -2\dot{h}/h$) can be integrated as $A_{zz}h^4 = h_0^4$. Differences in values of $(h_0/h_1)^4$ among the three polymer solutions are due to differences in h_1 stemming from different elastic moduli G , as we discuss in our longer companion paper [15] where we show that the Oldroyd-B model gives $h_1 \propto (GH^4/\gamma)^{1/3}$ where $H \rightarrow h_0$ for large relaxation times. We find in figure 4(b) that A_1 is very close to the $(h_0/h_1)^4$ limit for the PEO_{aq} and HPAM solutions at low h_0 , meaning that polymer relaxation

is indeed negligible, and that the ratio between the two increases as h_0 increases, meaning that relaxation becomes more important. This is consistent with the fact that the Deborah number $De = \tau_m/\tau_R$ decreases from 500 ($\gg 1$, i.e., negligible relaxation) at the lowest h_0 to 5 at the highest h_0 , where $\tau_R = \sqrt{\rho h_0^3/\gamma}$ is the Rayleigh time scale relevant for the thinning dynamics of such low-viscosity liquids, with Ohnesorge numbers $Oh = \eta_0/\sqrt{\rho\gamma h_0}$ which are up to 0.02 for PEO_{aq} and up to 0.1 for HPAM (at the lowest h_0 values), i.e. $Oh \ll 1$. The reason why the calculated values of A_1 are fairly independent of h_0 for these two liquids, hence resulting in an impossible match with the fitting values of A_1/L^2 (light purple) in figure 4(a), is therefore because these calculated values of A_1 are close to their upper limit $(h_0/h_1)^4$ which are fairly independent of h_0 themselves (at least for sufficiently low h_0 , see figure 4(b)). Note that the scaling $h_1 \propto h_0$ implied by the constant values of $(h_0/h_1)^4$ is discussed in our longer companion paper [15].

By contrast, the calculated values of A_1 for the PEO_{visc} solution are increasing as h_0 decreases, allowing for a good match with the fitting values of A_1/L^2 (light purple) in figure 4(a). This is because, unlike for the two other solutions, polymer relaxation (right hand side of equation 2) is not negligible in the Newtonian regime ($t < t_1$), as indicated by the greater difference between A_1 and the upper (relaxation-free) limit $(h_0/h_1)^4$ for the PEO_{visc} solution in figure 4(b). This is due to the slower thinning dynamics in the Newtonian regime, caused by a larger shear viscosity with Ohnesorge numbers $Oh = \eta_0/\sqrt{\rho\gamma h_0}$ ranging between 0.6 and 2 in our range of h_0 values. Indeed, since all three solutions have comparable relaxation times, slower thinning dynamics mean that polymer relaxation is more important, i.e., $A_1 < (h_0/h_1)^4$. The reason why A_1 decreases as h_0 increases for the PEO_{visc} solution is because the ratio between A_1 and $(h_0/h_1)^4$ increases with h_0 . This is because relaxation is increasingly important as h_0 increases since the time scale of the Newtonian thinning dynamics, expected to scale as $\tau_R \propto h_0^{3/2}$ or as $\tau_{\text{visc}} = \eta_0 h_0/\gamma \propto h_0$ depending on Oh , increases with h_0 , resulting in lower Deborah numbers (based on either τ_R or τ_{visc}).

4.5. Numerical simulations

Hence, The FENE-P model can only explain the increase of the apparent relaxation time τ_e with h_0 for the PEO_{visc} solution which is the most dilute one and with the highest solvent viscosity out of our three solutions. This is checked further by numerical simulations of the axisymmetric problem (with gravity) using the full FENE-P constitutive equation. We use as fixed model parameters the values of η_s and η_p from the shear rheology, the high- h_0 limit $\tau = \tau_m$ for the relaxation time and the value of $L^2 = 2.0 \times 10^4$ used in §4.4 (figure 4(a)) for which the simplified analytical model in §4.2 and §4.3 could rationalise the apparent relaxation times τ_e . The equations to be solved are the same as in Rubio et al [20] and the numerical methods are detailed in Appendix C. The initial condition is established by starting from a stable liquid bridge with a plate-to-plate distance L_p just below the instability

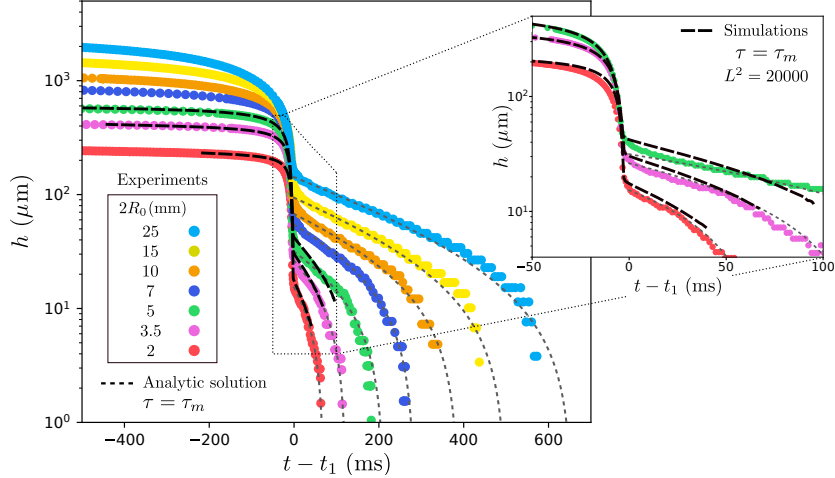


Figure 5: $h(t)$ from experiments and simulations for the PEO_{visc} solution for different plate diameters. Simulations are performed for $2R_0 = 2, 3.5$ and 5 mm only, using the FENE-P model with $\tau = \tau_m$ and $L^2 = 2.0 \times 10^4$. The elastic regime is fitted by equations 4 and 5 with $\tau = \tau_m$ where, like in figure 3(a), A_1/L^2 and h_1 are used as fitting parameters. The Ohnesorge numbers $Oh = \eta_0/\sqrt{\rho\gamma h_0}$ ranges between 2 and 0.6 for the PEO_{visc} solution in our range of h_0 values which corresponds to plates diameters $2R_0$ between 2 and 25 mm.

threshold value and slightly increasing L_p to trigger the pinch-off.

The results are shown in figure 5 for the three smallest plates and the corresponding experimental droplet volumes in terms of the time evolution of the minimum bridge / filament radius. Simulations are found to start at a bridge radius close to h_0 , which validates the numerical method to set the initial condition. We find that simulations are able to capture the Newtonian regime quite well and provide a reasonable agreement with experiments in the elastic regime. In particular, the filament thinning rate varies with the plate diameter, consistent with experiments, while the Oldroyd-B model would give the same (constant) thinning rate $1/3\tau_m$. Simulations could not be continued far enough to compare with the full experimental time window. Like in figure 3(a), figure 5 also features the analytic solution of equations 4 and 5 for the elastic regime ($t > t_1$).

5. Conclusions and discussion

We have shown experimentally that the thinning rate of filaments of various polymer solutions is not necessarily just a material property but may depend on the size of the system in CaBER with both slow (stepwise) and fast (step-strain) plate separation protocols as well as in DoS experiments, consistent with previous observations for dripping experiments [13]. Although all filaments are observed to thin exponentially, as predicted by the Oldroyd-B

model (see equation 1), we show that, for CaBER with slow stepwise plate separation, the inferred apparent relaxation time τ_e increases with the minimum bridge radius h_0 marking the onset of capillary thinning, which is an increasing function of both the plate diameter and droplet volume, and that τ_e saturates at large h_0 values corresponding to plate diameters > 10 mm significantly larger than typical CaBER plates. These observations hence suggest that CaBER relaxation times reported in the literature are not universal since testing a given polymer solution with different plate diameters and droplet volumes can yield significantly different results.

The fact that Bazilevsky et al. [1], who used both fast and slow-retraction CaBER methods, reported no variation of τ_e with the drop volume V (without providing the data to support their claim) might be due to the fact that its dependence on V is weak (weaker than its dependence on R_0 , see figure 2(a)) and that, for a given plate diameter, V can only be varied up to a critical value above which the drop does not fit on the plate.

We demonstrate that the variation of τ_e with h_0 is not caused by solvent evaporation or polymer degradation and cannot be universally explained by finite extensibility effects described by the FENE-P model. These observations suggest that the single-mode Oldroyd-B and FENE-P models miss some important features of polymer dynamics in extensional flows. The FENE-P model could only explain the variation of τ_e for the most dilute solution with the most viscous solvent, which is consistent with the fact that (i) the FENE-P model is derived for dilute solutions and that (ii) inertio-capillary oscillations are absent for this solution. However, since the value of the finite-extensibility parameter L^2 was chosen to optimise the agreement with experiments, we do not exclude that this agreement may also be a coincidence, although this value in agrees with the microscopic prediction (equation 6).

A physical interpretation for this deformation-history-dependent filament thinning rate is still needed, strengthening the already established need for better constitutive equations. Other shortcomings of the FENE-P model, such as coil-stretch hysteresis and the increase of τ_e with the polymer concentration in the ‘dilute’ regime ($c < c^*$), were previously explained by a Conformation-Dependent Drag (CDD) model accounting for the action of both chain stretching and intermolecular hydrodynamic interactions on the friction coefficient [21, 22]. Future works will determine if such models are also able to capture the system-size dependence of the effective relaxation time discussed in this paper.

Declaration of Interests. The authors report no conflict of interest.

Funding M. A. Herrada acknowledges funding from the Spanish Ministry of Economy, Industry and Competitiveness under Grant PID2022-140951O.

Acknowledgements. We thank Louison Laruelle and Carmen van Poelgeest for preliminary experimental work.

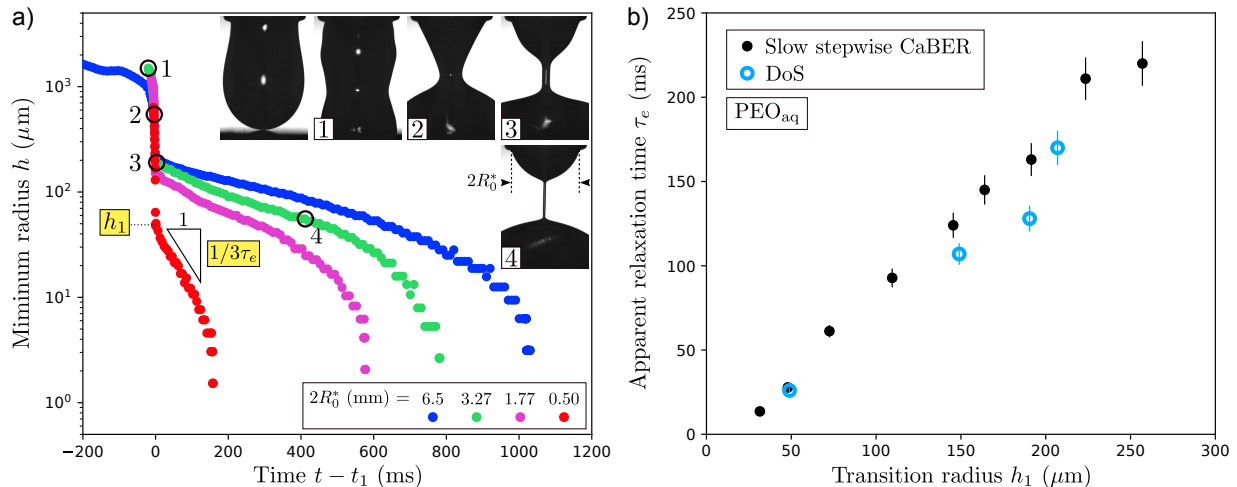


Figure A.6: (a) $h(t)$ from DoS experiments with different nozzle diameters for the PEO_{aq} solution. We report the values of the maximum diameter $2R_0^*$ of the top end-drop which is between the inner and outer nozzle diameter. Insert images correspond to the steadily hanging drop (left) and to four times labelled 1 to 4 indicated on the $h(t)$ curve for $2R_0^* = 3.27$ mm. (b) τ_e vs. h_1 for the PEO_{aq} solution from DoS compared to the values of figure 2(b) from CaBER with the slow stepwise plate separation protocol described in §2.2.

Appendix A. Dripping-onto-substrate (DoS)

In DoS experiments, a horizontal substrate (here, a plasma-treated aluminium plate) is moved slowly upward until being in contact with a liquid droplet hanging steadily from a nozzle. As shown in the image sequence in figure A.6(a), a fast spreading of the liquid on the plate leads to the pinch-off of the bridge connecting the substrate to the nozzle. This transiently leads to the formation of an exponentially thinning filament, as shown by the time-evolution of the minimum bridge / filament radius h in figure A.6(a), where the PEO_{aq} solution is tested with four different nozzle diameters. As in CaBER experiments, the apparent relaxation time extracted from the filament thinning rate increases with the droplet size, here quantified by the nozzle diameter. This apparent relaxation time τ_e is plotted in figure A.6(b) for both CaBER and DoS experiments against the filament radius h_1 marking the onset of the elastic regime which, unlike h_0 in CaBER, is easily definable in both methods. The relatively good collapse of the data points on a single curve suggests a universal physical mechanism for the dependence of the apparent relaxation time on the size of the system, independent of the exact method used. We checked that τ_e also increases with the nozzle diameter when the droplet spreads on a ‘small’ plate (about two times larger than the nozzle and made of non-plasma-treated aluminium), where spreading stops before the viscoelastic filament is formed.

$2R_0$ (mm)	Λ_0	Λ_f	t_f (ms)	$\dot{\epsilon}_0$ (s^{-1})	V^*
2	1.00	3.98	20	69.3	3.1
3.5	1.00	3.95	20	68.5	3.2
7	1.00	3.97	20	69.0	3.1
10	0.80	3.13	20	68.1	2.5
20	0.41	1.64	20	69.3	1.3

Table B.2: Parameters of experiments with the Haake CaBER-1 commercial extensional rheometer.

Appendix B. Step-strain CaBER

To further test the universality of the dependence of the apparent relaxation time on the system size, we also performed experiments with a Haake CaBER-1 commercial extensional rheometer (Thermo Haake GmbH, Karlsruhe, Germany) with plate diameters $2R_0$ between 2 and 20 mm. This was achieved by sticking aluminium plates of prescribed diameters to the 6 mm diameter plates provided with the rheometer where, as shown in figure B.7(d), the top plate was shortened to ensure that the total length would remain unchanged, allowing us to use the readings of the software to control the plate separation distance L_p . We chose an exponential plate separation profile of the form $L_p(t) = L_0 \exp(\dot{\epsilon}_0 t)$ with initial and final separation distances L_0 and L_f and with extension rate $\dot{\epsilon}_0 = t_f^{-1} \ln(L_f/L_0)$ where t_f is the duration of the separation profile. Values of these parameters are shown in table B.2 for each plate diameter where $\Lambda_0 = L_0/R_0$ and $\Lambda_f = L_f/R_0$ are the initial and final aspect ratios. The initial gap is filled by a nearly cylindrical liquid bridge, yielding a liquid volume $V \approx \pi R_0^2 L_0$ and a non-dimensional liquid volume $V^* = V/R_0^3 \approx \pi \Lambda_0$ given in table B.2. We choose $\Lambda_0 = 1$ for the smallest plates, consistent with Miller et al. [12], and lower values for the largest plates for which, due to gravity, it was no longer possible to fit the sample in a $\Lambda_0 = 1$ initial gap. We keep the final-to-initial distance L_f/L_0 close to 4 and choose the smallest available strike time $t_f = 20$ ms to maximise the extension rate $\dot{\epsilon}_0 \approx 69 \text{ s}^{-1}$ and hence the Weissenberg number $Wi_0 = \tau \dot{\epsilon}_0$ which, since the apparent relaxation times about to be discussed are larger than 30 ms, is larger than 2 and therefore within the range considered by Miller et al. [12]. This ensures that polymer chains do not relax during the (hence rightfully named) initial step-strain or step-stretch. Experiments of Miller et al. [12] for a fixed plate diameter $2R_0 = 3$ mm and initial aspect ratio $\Lambda_0 = 1$ showed that the (apparent) relaxation time τ_e (inferred from the exponential thinning regime) doesn't depend on the step-strain parameters Λ_f (varied between 3 and 15) and Wi_0 (varied between 0.5 and 12) for polymer solutions.

We used the PEO_{aq} and PEO_{visc} solutions of figure 2(b) that we label here $\text{PEO}_{\text{aq,old}}$ and $\text{PEO}_{\text{visc,old}}$ since they were about 7 months old by the time we tested them on the

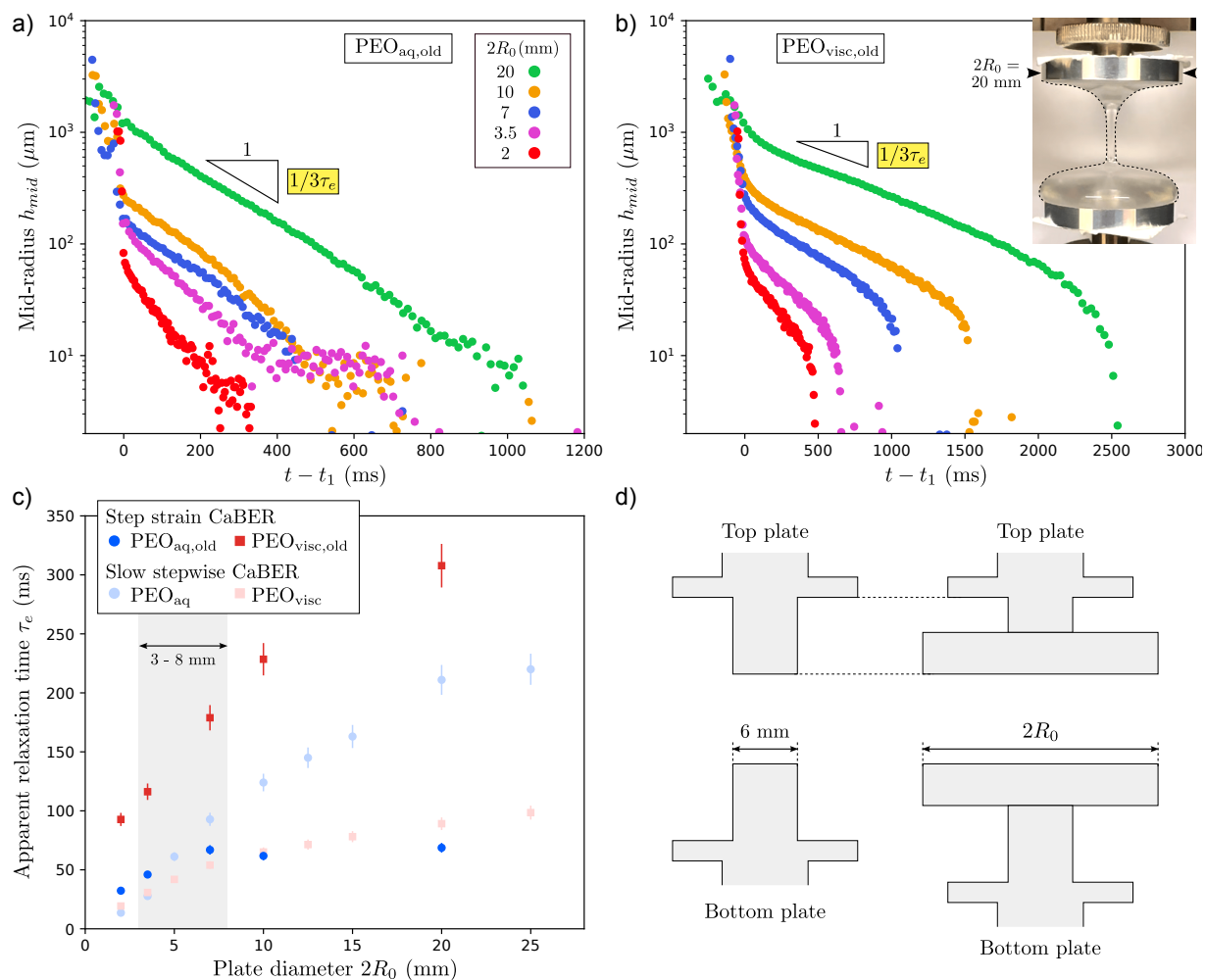


Figure B.7: (a,b) Time evolution of the mid-filament radius $h_{mid}(t)$ for the $\text{PEO}_{\text{aq,old}}$ (a) and $\text{PEO}_{\text{visc,old}}$ (b) solutions tested with plate diameters $2R_0 = 2, 3.5, 7, 10$ and 20 mm on a Haake CaBER-1 extensional rheometer. The time t_1 corresponds to the onset of the exponential regime. The legend is the same for both figures and the inset picture in (b) shows an example of thinning filament for the $\text{PEO}_{\text{visc,old}}$ solution tested with the 20 mm diameter plates, the air-liquid interface being highlighted with dashed lines. (c) Apparent relaxation time τ_e against the plate diameter with, for reference, the values from figure 2(b) for the PEO_{aq} and PEO_{visc} solutions tested with the slow stepwise plate separation protocol described in §2.2. The shaded area corresponds to the range of plate diameters $3 - 8$ mm available for a Haake CaBER-1 extensional rheometer. (d) Sketch of the original (left) and modified (right) design allowing for a change in plate diameter.

Haake CaBER-1 rheometer compared to when they were tested with the slow stepwise plate separation protocol. The time evolution of the mid-filament radius h_{mid} measured by the laser micrometer is shown in figures B.7(a) for the $\text{PEO}_{\text{aq,old}}$ solution and in figure B.7(b)

for the $\text{PEO}_{\text{visc,old}}$ solution for all plate diameters. The relaxation time τ_e inferred from the exponential part of the thinning dynamics, calculated from the filament thinning rate $|\dot{h}/h|$ defined as $1/3\tau_e$, is plotted against the plate diameter in figure B.7(c) for both liquids. We find that τ_e increases significantly as the plate diameter increases for the $\text{PEO}_{\text{visc,old}}$ solution. For the $\text{PEO}_{\text{aq,old}}$ solution, τ_e increases by a factor 2 for $2R_0$ between 2 and 7 mm and reaches a plateau for $2R_0 \geq 7$ mm. This initial increase is not caused by experimental error, as indicated by the small error bars estimated by repeating the experiment three times for each plate. These results confirm that the apparent relaxation time increases with the plate diameter regardless of whether the plates are separated slowly or rapidly in CaBER. The range of plate diameters 3 – 8 mm used with the Haake CaBER-1 rheometer is shown in grey in figure B.7(c) to emphasise that, generally speaking, there is no reason to consider any apparent relaxation time measured in this range as ‘the’ relaxation time.

The apparent relaxation times of figure 2(b), measured with the slow stepwise plate separation CaBER protocol described in §2.2, are shown in figure B.7(c) for reference. Values of τ_e are in general lower for the $\text{PEO}_{\text{aq,old}}$ solution compared to the PEO_{aq} (fresh) one, consistent with the expected ageing of the solution over the 7 months separating the two sets of experiments which was confirmed by shear rheology experiments revealing a 29% decrease in η_0 . On the other hand, values of τ_e are found to be higher for the $\text{PEO}_{\text{visc,old}}$ compared to the PEO_{visc} (fresh) one. The (constant) shear viscosity was also found to be higher by about 24% which, since $\eta_s \gg \eta_p$, can be explained by an increase in the solvent viscosity which cannot be caused by evaporation since the solution was sealed. A possible explanation could be the development of microorganisms. The change in apparent relaxation times is therefore not necessarily caused by the change in plate separation protocol, consistent with Bazilevsky et al. [1] who found no significant difference in τ_e for solutions tested with both slow and fast protocols.

Appendix C. Numerical method

The FENE-P model was solved with a variation of the method described by Herrada & Montanero [23]. The physical domains occupied by the liquid is mapped onto a rectangular domain through a coordinate transformation. Each variable and its spatial and temporal derivatives appearing in the transformed equations were written as a single symbolic vector. Then, we used a symbolic toolbox to calculate the analytical Jacobians of all the equations with respect to the symbolic vector. Using these analytical Jacobians, we generated functions that could be evaluated in the iterations at each point of the discretised numerical domains.

The transformed spatial domain is discretised using $n_\eta = 11$ Chebyshev spectral collocation points in the transformed radial direction. We used $n_\xi = 801$ equally spaced collocation points in the transformed axial direction ξ . The axial direction was discretised using fourth-order finite differences. Second-order backward finite differences were used to discretise the

time domain. We used an automatic variable time step based on the norm of the difference between the solution calculated with a first-order approximation and that obtained from the second-order procedure. The nonlinear system of discretised equations was solved at each time step using the Newton method. The method is fully implicit.

References

- [1] A. Bazilevsky, V. Entov, M. Lerner, A. Rozhkov, Failure of polymer solution filaments, *Polymer Science-Series A* 39 (3) (1997) 316–324.
- [2] S. L. Anna, G. H. McKinley, Elasto-capillary thinning and breakup of model elastic liquids, *Journal of Rheology* 45 (1) (2001) 115–138.
- [3] M. Stelter, G. Brenn, A. Yarin, R. Singh, F. Durst, Validation and application of a novel elongational device for polymer solutions, *Journal of Rheology* 44 (3) (2000) 595–616.
- [4] L. E. Rodd, T. P. Scott, J. J. Cooper-White, G. H. McKinley, Capillary break-up rheometry of low-viscosity elastic fluids, *Applied Rheology* 15 (1) (2005) 12–27.
- [5] L. Campo-Deano, C. Clasen, The slow retraction method (SRM) for the determination of ultra-short relaxation times in capillary breakup extensional rheometry experiments, *Journal of Non-Newtonian Fluid Mechanics* 165 (23-24) (2010) 1688–1699.
- [6] V. Tirtaatmadja, G. H. McKinley, J. J. Cooper-White, Drop formation and breakup of low viscosity elastic fluids: Effects of molecular weight and concentration, *Physics of fluids* 18 (4) (2006) 043101.
- [7] J. Dinic, L. N. Jimenez, V. Sharma, Pinch-off dynamics and dripping-onto-substrate (dos) rheometry of complex fluids, *Lab on a Chip* 17 (3) (2017) 460–473.
- [8] A. Bazilevsky, V. Entov, A. Rozhkov, Liquid filament microrheometer and some of its applications, in: *Third European Rheology Conference and Golden Jubilee Meeting of the British Society of Rheology*, Springer, 1990, pp. 41–43.
- [9] V. M. Entov, E. J. Hinch, Effect of a spectrum of relaxation times on the capillary thinning of a filament of elastic liquid, *Journal of Non-Newtonian Fluid Mechanics* 72 (1) (1997) 31–53.
- [10] C. Clasen, J. Eggers, M. A. Fontelos, J. Li, G. H. McKinley, The beads-on-string structure of viscoelastic threads, *Journal of Fluid Mechanics* 556 (2006) 283–308.
- [11] C. Clasen, J. P. Plog, W.-M. Kulicke, M. Owens, C. Macosko, L. E. Scriven, M. Verani, G. H. McKinley, How dilute are dilute solutions in extensional flows?, *Journal of Rheology* 50 (6) (2006) 849–881.

- [12] E. Miller, C. Clasen, J. P. Rothstein, The effect of step-stretch parameters on capillary breakup extensional rheology (CaBER) measurements, *Rheologica acta* 48 (2009) 625–639.
- [13] S. Rajesh, V. Thiévenaz, A. Sauret, Transition to the viscoelastic regime in the thinning of polymer solutions, *Soft Matter* 18 (16) (2022) 3147–3156.
- [14] L. A. Slobozhanin, J. M. Perales, Stability of liquid bridges between equal disks in an axial gravity field, *Physics of Fluids A: Fluid Dynamics* 5 (6) (1993) 1305–1314.
- [15] A. Gaillard, M. Herrada, A. Deblais, C. van Poelgeest, L. Laruelle, J. Eggers, D. Bonn, When does the elastic regime begin in viscoelastic pinch-off?, *arXiv preprint arXiv:2406.02303* (2024).
- [16] C. Wagner, L. Bourouiba, G. H. McKinley, An analytic solution for capillary thinning and breakup of FENE-P fluids, *Journal of Non-Newtonian Fluid Mechanics* 218 (2015) 53–61.
- [17] J. Eggers, M. A. Herrada, J. Snoeijer, Self-similar breakup of polymeric threads as described by the Oldroyd-B model, *Journal of fluid mechanics* 887 (2020) A19.
- [18] A. Bazilevsky, V. Entov, A. Rozhkov, Breakup of an Oldroyd liquid bridge as a method for testing the rheological properties of polymer solutions, *Polymer Science Series AC/C of Vysokomolekuliarnye Soedineniia* 43 (7) (2001) 716–726.
- [19] J. Brandrup, E. H. Immergut, *Polymer Handbook*, John Wiley & Sons, New York, 1999.
- [20] M. Rubio, E. J. Vega, M. A. Herrada, J. M. Montanero, F. J. Galindo-Rosales, Breakup of an electrified viscoelastic liquid bridge, *Physical Review E* 102 (3) (2020) 033103.
- [21] R. Prabhakar, S. Gadkari, T. Gopesh, M. Shaw, Influence of stretching induced self-concentration and self-dilution on coil-stretch hysteresis and capillary thinning of unentangled polymer solutions, *Journal of Rheology* 60 (3) (2016) 345–366.
- [22] R. Prabhakar, C. Sasmal, D. A. Nguyen, T. Sridhar, J. R. Prakash, Effect of stretching-induced changes in hydrodynamic screening on coil-stretch hysteresis of unentangled polymer solutions, *Physical Review Fluids* 2 (1) (2017) 011301.
- [23] M. Herrada, J. M. Montanero, A numerical method to study the dynamics of capillary fluid systems, *Journal of Computational Physics* 306 (2016) 137–147.